

# Dynamic superconcentration at critical-point double-layer gates of conducting nanoporous granules due to asymmetric tangential fluxes

Shau-Chun Wang,<sup>1</sup> Hsien-Hung Wei,<sup>2</sup> Hsiao-Ping Chen,<sup>1</sup> Min-Hsuan Tsai,<sup>1</sup> Chun-Ching Yu,<sup>1</sup> and Hsueh-Chia Chang<sup>3</sup>

<sup>1</sup>*Department of Chemistry and Biochemistry, National Chung Cheng University, Chia-Yi 621, Taiwan*

<sup>2</sup>*Department of Chemical Engineering, National Cheng Kung University, Tainan 701, Taiwan*

<sup>3</sup>*Department of Chemical and Biomolecular Engineering, University of Notre Dame, Notre Dame, Indiana 46556, USA*

(Received 21 January 2008; accepted 7 March 2008; published online 31 March 2008)

A transient  $10^6$ -fold concentration of double-layer counterions by a high-intensity electric field is demonstrated at the exit pole of a millimeter-sized conducting nanoporous granule that permits ion permeation. The phenomenon is attributed to a unique counterion screening dynamics that transforms half of the surface field into a converging one toward the ejecting pole. The resulting surface conduction flux then funnels a large upstream electro-osmotic convective counterion flux into the injecting hemisphere toward the zero-dimensional gate of the ejecting hemisphere to produce the superconcentration. As the concentrated counterion is ejected into the electroneutral bulk electrolyte, it attracts co-ions and produce a corresponding concentration of the co-ions. This mechanism is also shown to trap and concentrate co-ion microcolloids of micron sizes too (macroions) and hence has potential application in bead-based molecular assays. © 2008 American Institute of Physics.

[DOI: [10.1063/1.2904640](https://doi.org/10.1063/1.2904640)]

## I. INTRODUCTION

Field-induced polarization of particles and molecules is responsible for a variety of electric particle and molecular forces that permit particle manipulation,<sup>1</sup> drive colloid self-assembly,<sup>2</sup> and allow suspension characterization.<sup>3</sup> Conventional Maxwell-Wagner theories attribute these electric induced dipoles to interfacial dielectric polarization that occurs at atomic, molecular, and particle times and length scales, and exhibit megahertz or higher dispersion frequencies.<sup>4</sup> In electrolytes, there is considerable evidence that double-layer conduction around the particle,<sup>5–7</sup> normal charging into the double layer of thickness  $\lambda$ ,<sup>8–10</sup> and other polarization mechanisms involving currents, ion fluxes, electro-osmotic convection, and charge storage in double layers<sup>11,12</sup> are the more dominant polarization mechanisms than dielectric polarization. These double-layer polarization mechanisms are confined to the thin double layers (of 10–100 nm) but nevertheless involve space charges. Empirical evidence for such double-layer polarization mechanisms includes the prevalence of the relaxation time  $a\lambda/D$  in many impedance and dielectrophoresis measurements<sup>7</sup> which requires a conducting Stern layer.<sup>5,7,12</sup> However, these lumped conductivity models do not capture local charge accumulation (capacitance) effects at certain locations within the double layer, which will be shown to occur in this paper.

Indeed, recent ion transport studies of nanoporous material and nanochannels<sup>13,14</sup> suggest that conduction (and charge storage) in the nanometer-sized double layers or pores can produce local charge buildup within the double layer. The experiment by Leinweber and Tallarek,<sup>14</sup> for example, shows that in the presence of a strong applied field, the fluorescent counterions exiting from a nanoporous spherical granule remain confined to the double layer on the granule surface. These

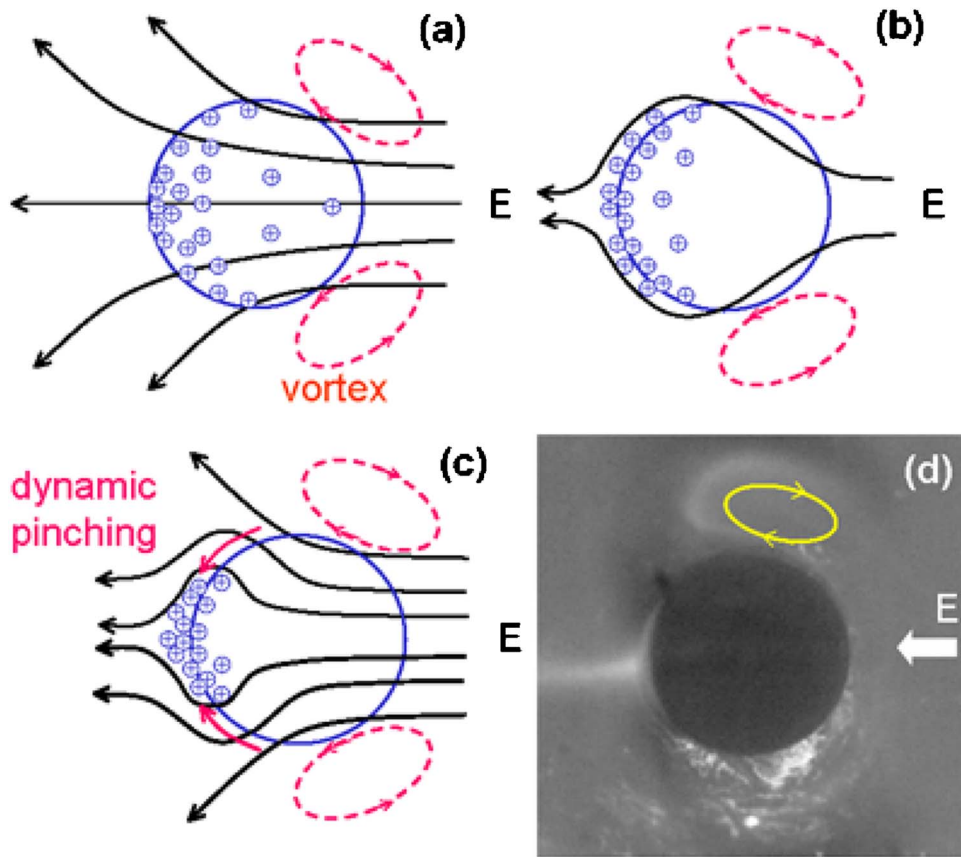


FIG. 1. The granule funnel: (a) Convective charging of the granule by asymmetric vortices at the right, (b) saturation of the double layer by counterions exiting the granule and field screening, and (c) dynamic double-layer pinching toward the ejection pole. (d) is a real image showing the polar ejection and the asymmetric vortices on the other hemisphere. One vortex evidenced from the dye streaks is highlighted. (The white areas in the images in Figs. 1 and 3 are due to scattering light reflected from a coarse surface.)

confined counterions have a nonuniform concentration on the granule surface that peaks at ten times that of the bulk at one pole, where the applied field penetrates axially through the granule. Such local dynamic charging and gating effects at the poles are expected to induce intense dipole moments that can produce anomalous dielectrophoretic behavior with new relaxation time signatures in the dielectric or impedance spectra, and allow for the concentration of space charges for analytical applications.<sup>15</sup>

In this paper, we examine the mechanism behind the transient ion concentration phenomenon at the polar gate and demonstrate that a six-order enhancement in the ion concentration can be achieved locally within the double layer if the granule is permeable to ions, with a comparable enhancement of Maxwell-Wagner polarization. We image the enhanced counterion concentration not by the counterions dye molecules, which are too large to enter the nanopores, but by fluorescent co-ion dye molecules which neutralize the counterions at the exit of the granule and whose concentration is correspondingly enhanced at that location.

To concentrate space charges within the double layer at the gate, a converging tangential flux from the granule toward the pole must be implemented as normal charging into this small polar region is insignificant. The requisite tangential field at the ejection hemisphere is produced by the screening effects of the exiting counterions from the saturated granule, as seen in Fig. 1. A tangential counterion flux results at the ejecting hemisphere that must be sustained by an equally large tangential flux at the injecting hemisphere under the condition when the granule is permeable and cannot accumulate ions. Consequently, ion fluxes into and out of the granule are required for

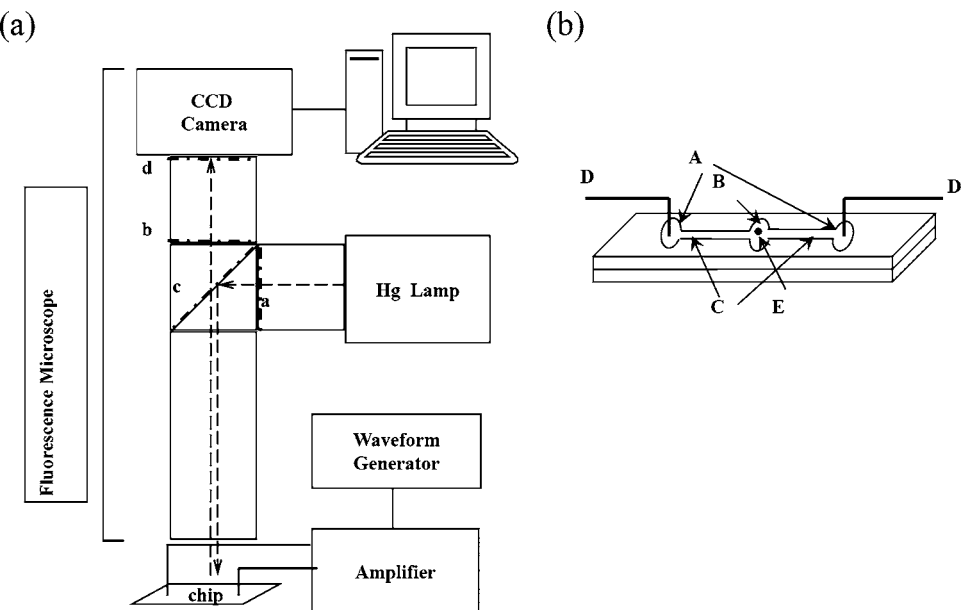


FIG. 2. (a) Schematic chart of the fluorescence microscopy imaging apparatus. a, excitation filter; b, emission filter; c, dichromatic mirror; d, 510–530 nm bandpass filter. (b) Illustration of the imaging chip in detail. A, side reservoirs; B, center reservoir; C, connection channels; D, platinum electrodes; E, cation exchange granule.

large polar concentration. As a general rule, pores with radii smaller than  $\lambda$  tend to trap large amounts of counterions and would not release them to the exit hemisphere.<sup>13</sup> This important pore size effect for superconcentration will be established in our experiments.

The possibility of concentrating microcolloids which are larger than the double layer dimension is an intriguing possibility. The microcolloids are not expected to enter into the granule. However, co-ion microcolloids can still be attracted to the concentrated counterions at the exit. Bead-based biomolecular assays<sup>16</sup> have attracted considerable attention recently and the possibility of filtering and concentrating such functionalized or hybridized beads on a chip can be quite useful for such assays.

## II. EXPERIMENTAL

Fluorescein sodium salt obtained from Riedel-de Haën is dissolved in Tris buffer (1.0 M) to prepare the standard solution of anionic dyes at the concentrations 0.02, 0.20, 2.0, 20, 200, 2000,  $1.0 \times 10^4$ , and  $1.0 \times 10^5$   $\mu\text{M}$ . The standard solution of varied concentration is filled into the device reservoir and illuminated with the fluorescence microscopy apparatus (SMZ1500, Nikon). The emitted fluorescence is detected with a charge-coupled device (CCD) camera (WAT-902H, Watec, Japan) at the frame rate 30 Hz for 1 s. The images are collected and the CCD signal intensities at each pixel are averaged. The fluorescence intensity is determined by the difference between the full gray scale of CCD (255) and the average scale detected with the CCD at the reservoir area. This difference value is defined as the inverted gray scale. Rhodamine B from Sigma is used to prepare the standard solution of cationic dyes.

Figure 2 shows a schematic chart of our apparatus. We use millimeter-sized commercial conducting granules made of polystyrene resins (Lewatit K-2629, Bayer) in our experiments. Literature values<sup>17</sup> indicate the pore size to be 65 nm, or roughly to 3–5 times the double-layer thickness of our more concentrated buffers ( $>0.1$  mM). The conducting granule is placed at a reservoir 0.15 cm in radius and 10  $\mu\text{l}$  in volume. An external electric field of about 100 V/cm is applied on the granule by a pair of electrodes (3 cm in separation and housed in side channels of the reservoir) using a power amplifier (Model 10/10B, Trek, NY) and a functional generator (Agilent). The granule can be either negatively charged (cation exchange) or positively charged

(anion exchange). Fluorescence dye solution of cation (Rhodamine B) or anion (fluorescein) at concentrations of 1 to 20  $\mu\text{M}$  in 10 mM pH buffers is filled in the reservoir prior to the field application. The granule is either completely or partially submerged in an electrolyte, with the latter configuration allowing for the imaging of the migrating fluorescent dye in profile. As described in the Introduction, net charges (mostly counterions) released from the granule are immediately neutralized by co-ions in the bulk in a region close to the granule. Since we employed co-ions as fluorescent dyes to illuminate the phenomenon, the ejection reflects a local increase in the concentration in the neutral bulk close to the granule. The chip is housed under the lens of a fluorescence microscope (SMZ1500, Nikon) with mercury lamp light source. A CCD camera (WAT-902H, Watec, Japan) is used to record the images of the process. The images are digitized and transferred into graphic analysis software.

Fluorescein-tagged anionic microspheres (latex particles at 1  $\mu\text{m}$ ) are filled into the reservoir for the microcolloid trapping experiments. The dye molecules render the microcolloids negatively charged and are hence expected to behave like fluorescein dye molecules with a lower mobility. These microcolloids are illuminated with the same fluorescence microscope setup. The trapping dynamics are recorded with electron-multiplying CCD (iXon, Andor).

### III. RESULTS AND DISCUSSION

The relation of the inverted gray scale versus the logarithm value of fluorescein concentration is recorded. Fluorescein fluorescence intensity becomes saturated when its concentration is 0.01  $\mu\text{M}$  or higher. The intensity no longer scales linearly with respect to the dye concentration in the concentration range of the above standard solutions. The fluorescence intensity gradually saturates when the concentration increases. Therefore, the regression results show a linear relation  $Y=220.5+22.3X$ , where  $Y$  and  $X$  are the inverted gray scale and the logarithm value of fluorescein concentration, respectively. The correlation coefficient of this regression curve is 0.996. A similar logarithm relation between fluorescence intensity and logarithm of dye concentration is found in the paper by Wang and co-workers.<sup>15</sup>

Sequential frames in Fig. 3 show the evolution of co-ion (fluorescein) concentration processes under a step jump in the field strength 100 V/cm for the negatively charged granule with positive counterions in the double layer. During this process, the lapsed frames capture the concentration of the anion dye, which is a co-ion, toward the ejecting hemisphere to form a distinctive rim. The rim then focuses toward the exit pole close to the negative electrode, with a migration time of about 1 s. Upon reaching the pole, the dye concentrates and emits an intense fluorescent glow for an interval of 0.3 s before a violent ejection in the form of a jet occurs in Fig. 3(d) at 0.93 s. The pinching of the rim toward the pole, as sketched in Fig. 1 to demonstrate the appearance of tangential field and flux, is evident in the images. In addition, owing to space-charge buildup in the double layer on the injecting hemisphere, the observed pinching phenomenon is accompanied with a pair of microvortices behind the rim, as shown in Fig. 1(d).

The thickness of the pole region with the concentrated dye is estimated to be about 100  $\mu\text{m}$ , much larger than the estimated double-layer thickness of  $\lambda=10$  nm. That the co-ion dye concentrates near the particle and migrates toward the exit pole indicates that there is a thicker electro-neutral sublayer with large concentration gradients and, more importantly, the co-ion dynamics in the thick sublayer mirror that of the counterion in the much thinner and invisible double layer. As conjectured in Fig. 1, the counterions must have migrated out of the granule to attract a rim of co-ions in the ejecting hemisphere, and must have focused toward the pole, as the tracking fluorescent co-ions indicate in Fig. 3.

By subtracting the blank background (10 mM Tris buffer; pH 8) and correlating the reduced pixel intensity to the dye concentration, the evolving dye concentration field can be quantitatively estimated. The intensities at the most concentrated spot (the exit pole position) and the ejecting jet area are measured as about  $\sim 10^6$  and  $\sim 10^5$  times greater, respectively, than that at the homogenized area immediately before the ejection (Fig. 4). To underscore that ion permeation into the granule is necessary for this  $10^6$ -fold dynamic superconcentration, which was not observed in earlier steady-state experiments with smaller pores,<sup>14</sup> we have carried out experiments at various

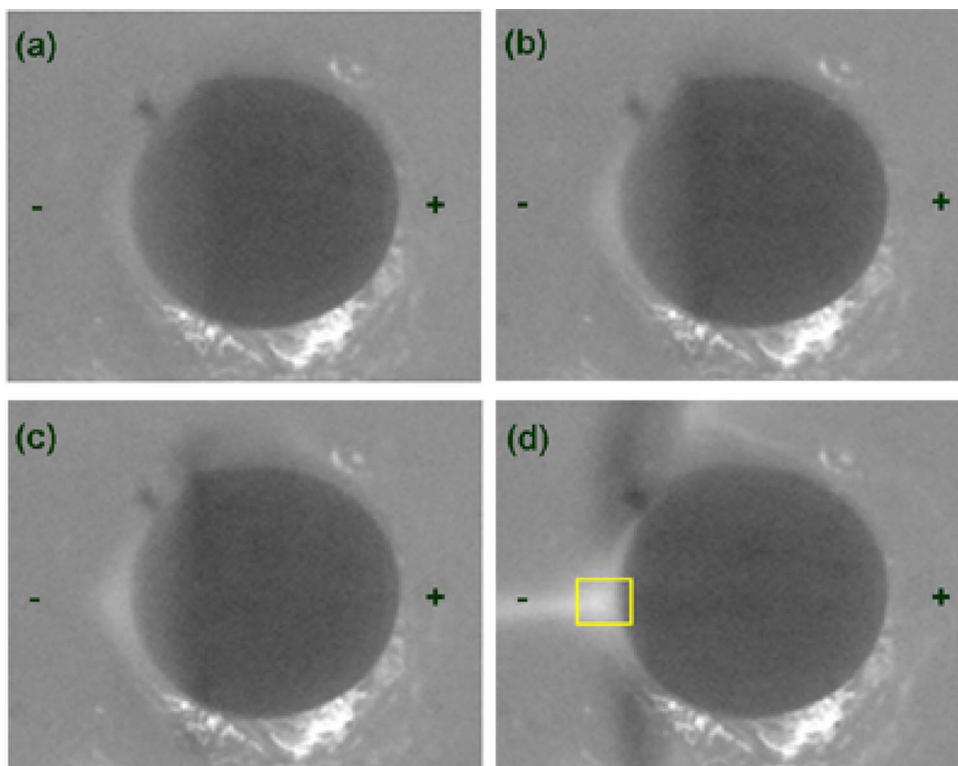


FIG. 3. The sequential images of solute concentration evolution for a cation exchange granule with a step change in the field to 100 V/cm using co-ion fluorescein dyes (20  $\mu\text{M}$  in 10 mM Tris buffer at pH 8). The images are taken at 0, 0.36, 0.63, and 0.93 s. (d) is an enlargement of Fig. 1(d).

ionic strengths and with a wax bead of similar dimension. As seen in Fig. 5, the enhancement factor drops precipitously by one to two orders of magnitude at a concentration 0.1 mM, when the Debye length is estimated to be 30 nm and expected to be comparable to our pore size. There is no enhancement at all for the wax bead without any pores. The higher conductivity data from 3 to 10 mM produce the  $\sim 10^5$ -fold concentration, suggesting the importance of permeation. When the Debye length is approximately equal to the pore size, the surface field is not screened and counterions with affinity for the surface functional groups condense readily onto the surface. As a consequence, the influx counterions are no longer able to migrate through the pore and therefore are captured within the granule.

A similar co-ion concentration in the bulk region near the pole is observed when a positively charged granule is used with cationic dye Rhodamine B (Fig. 6). Anionic counterions are absorbed onto the exit hemisphere to form a rim, which focuses toward the pole and ejects after a delay. The polar concentration and ejection phenomena are symmetric with respect to the granule and double-layer polarity.

Similarly when a negatively charged granule is in the reservoir, the trapping of anionic microspheres tagged with fluorescein dyes is seen. Figure 7 shows fluorescein-tagged particles at very low density ( $5.0 \times 10^6$  particles/mL) are concentrated at the granule exit pole. The concentrated particle density is estimated as  $1.5 \times 10^8$  particles/mL. As high as a 30-fold concentration of the microcolloids is recorded despite their large dimension relative to the double layer and their low mobility, and despite the fact that the microcolloids do not enter or exit the granule. The reflection of the incoming light by the microspheres is much stronger than scattered light from the reservoir bottom in Figs. 1 and 3, thus preventing the latter from contaminating the image.

It is clear from the images that a large concentration gradient exists along the granule surface to produce the large concentration at the pole. This is attributed to the imbalance between three

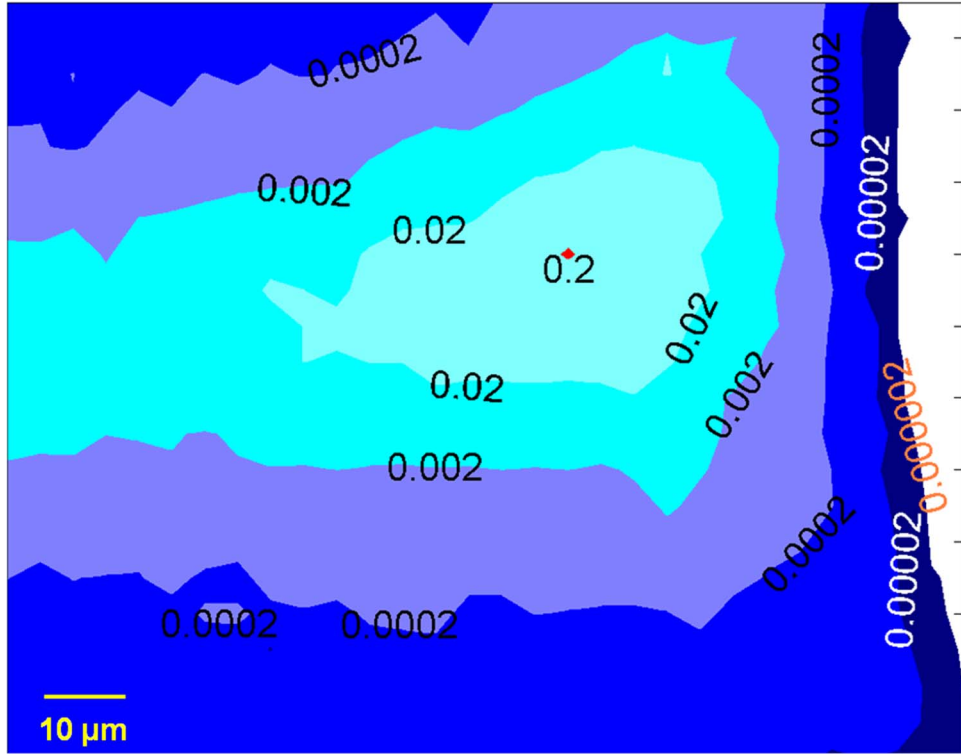


FIG. 4. The concentration intensity contour in the region highlighted in Fig. 3(d). The numbers on the concentration contour map indicate estimated molar concentration of the dye. The white area at the right side of the contour is the granule edge marked in the yellow frame of Fig. 3(d). The concentration is enhanced by  $\sim 10^6$  and  $\sim 10^5$  times the bulk value at the most concentrated spot and the jet area, respectively.

tangential fluxes in the presence of an electric field  $E$ : diffusion  $(D/a)(\partial C/\partial \theta)$ , electromigration  $E(DF/RT)C$  and convection  $UC$  (where  $\theta$  is the azimuthal angle,  $R$  the gas constant,  $F$  the Faradaic constant, and  $T$  the temperature). Here, the electro-osmotic velocity is  $U = -\varepsilon\zeta E/\mu$ , with  $\zeta$  the natural or induced zeta potential,  $\varepsilon$  the permittivity, and  $\mu$  the viscosity. We also use two dimensionless parameters  $\Gamma = FEA/RT$  and the Péclet number  $Pe = Ua/D$  to measure the relative magnitudes of electromigration and convection to diffusion, respectively. In particular, the electromigration time around the exit hemisphere, where there is little convective contribution, is  $a^2/(\Gamma D) \sim aRT/(FDE)$ , which is about 1 s for conditions in Fig. 3 and is consistent with our experimental observation of the front migration time.

As the normal counterion flux on the granule side is much weaker than the same flux on the electrolyte side on the injecting hemisphere, Dukhin<sup>5</sup> first suggested that there is significant space charge, i.e., mobile ions, buildup in the double layer on the injecting hemisphere, whose screening effect also renders the surface field of the injecting hemisphere more tangential [see Fig. 1(a)]. This double-layer polarization due to normal charging of the granule produces a large effective zeta potential  $\zeta$  on the order of  $Ea$  and the nonuniformity of the polarization produces an intense vortex pair at the injection hemisphere<sup>5,11</sup> [see Fig. 1(d)]. In our earlier study,<sup>11</sup> we have shown that this intense vortex pair can exhibit a tangential velocity as high as 1 cm/s for a 1-mm granule when the dimensionless field  $\Gamma = FEA/RT$  reaches 100. The corresponding Péclet number  $Pe = Ua/D$  at the injecting hemisphere is as high as  $10^4$ , so electro-osmotic convection dominates the tangential transport therein. This strong convection creates a diffusion boundary layer of thickness  $l = a/Pe^{1/2}$  near the surface,<sup>11</sup> rendering a large convective tangential flux within it. Since the asymmetric vortex pair only exists on the side of the injecting hemisphere, the tangential flux mechanism changes from convection to electromigration at the equator, such that the flux velocity

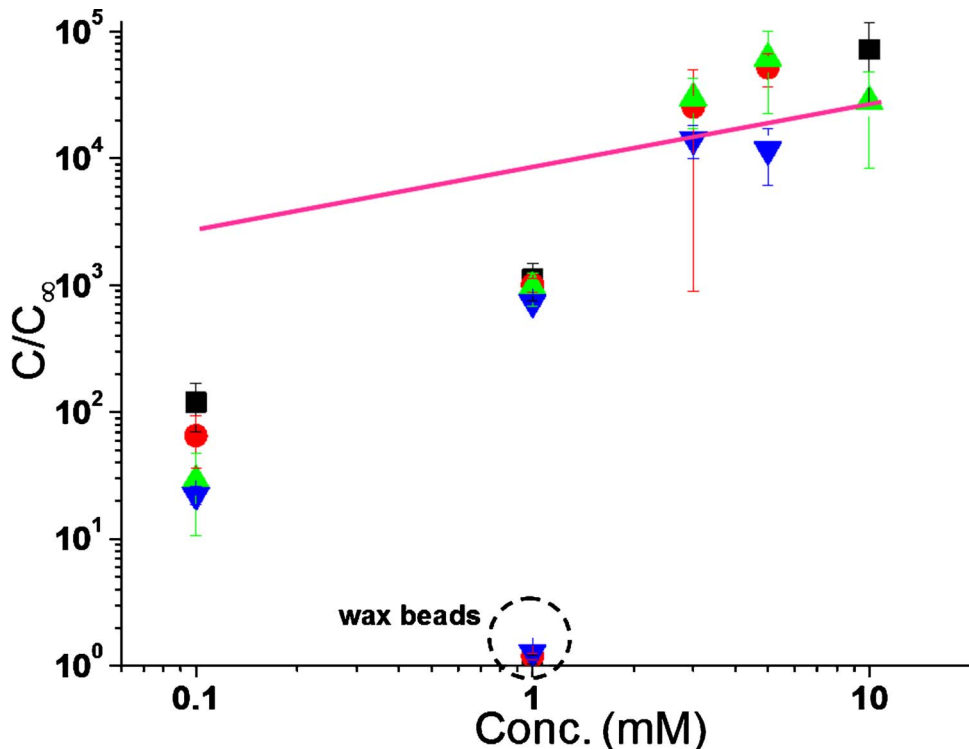


FIG. 5. The measured concentration factor in the jet area at different ionic strengths (buffer concentrations) and for wax beads. (67 V/cm, ■; 100 V/cm, ●; 115 V/cm, ▲; 133 V/cm, ▼). The slope of the line is 0.5, as the predicted enhancement is inversely proportional to the Debye length. (The Debye length is inversely proportional to the square root of the electrolyte concentration.) The points in the dashed circle are obtained using a wax bead.

ratio reduces by  $(\Gamma/\text{Pe})$  and the flux area ratio also changes by a factor of  $(\lambda/l)$ . Hence, to maintain a constant total flux, the concentration must increase downstream in the ejecting jet area by a factor of  $(\text{Pe}^{1/2}/\Gamma)(a/\lambda)$  or  $(\varepsilon/\mu D)^{1/2}(RT/F)(a/\lambda)$ .

The above argument corresponds to the counterion concentration. However, when the concentrated ions are ejected from the pole, they attract co-ions to achieve neutrality. In fact, both the co-ion tagged microcolloids and the large co-ion fluorescent dye molecules are probably not the ones being concentrated via transit through the granule and tangential surface flux toward the pole. Rather, it is a smaller counterion that is so concentrated with the larger co-ion simply tracking the enhanced counterion concentration as the latter ions exit the double layer into the electroneutral bulk. This is why only the co-ion dye or co-ion dye tagged microcolloids are concentrated by the ion-exchange granules.

While the larger granules render the greater concentration enhancement, there is an added advantage using larger (millimeter-sized) granules. The surface electromigration time  $a^2/(TD) \sim aRT/(FDE)$  for these larger granules is the order of seconds, hence allowing the phenomenon to be monitored by typical fluorescence video speeds.

In addition, the large value of  $\Gamma = FEA/RT$  stipulates that diffusion is unimportant except in a small neighborhood around the hyperbolic critical point of the electric field at the exit pole, where the field and tangential electromigration flux both approach zero. Near this critical point, the field grows as  $E(\delta/a)$  radially away from the fixed point, where  $\delta$  is the linear distance from the critical point and also measures the lateral and normal dimension of the pole region. Through a simple balance between electromigration and diffusion fluxes near the exit pole, we find  $\delta \sim a/\sqrt{\Gamma}$ , which is roughly 100  $\mu\text{m}$  for the conditions in the experiments. The bar in Fig. 8 is of length  $\delta$  and is consistent in magnitude with the thickened polarized layer at the pole captured by our fluoresced image.

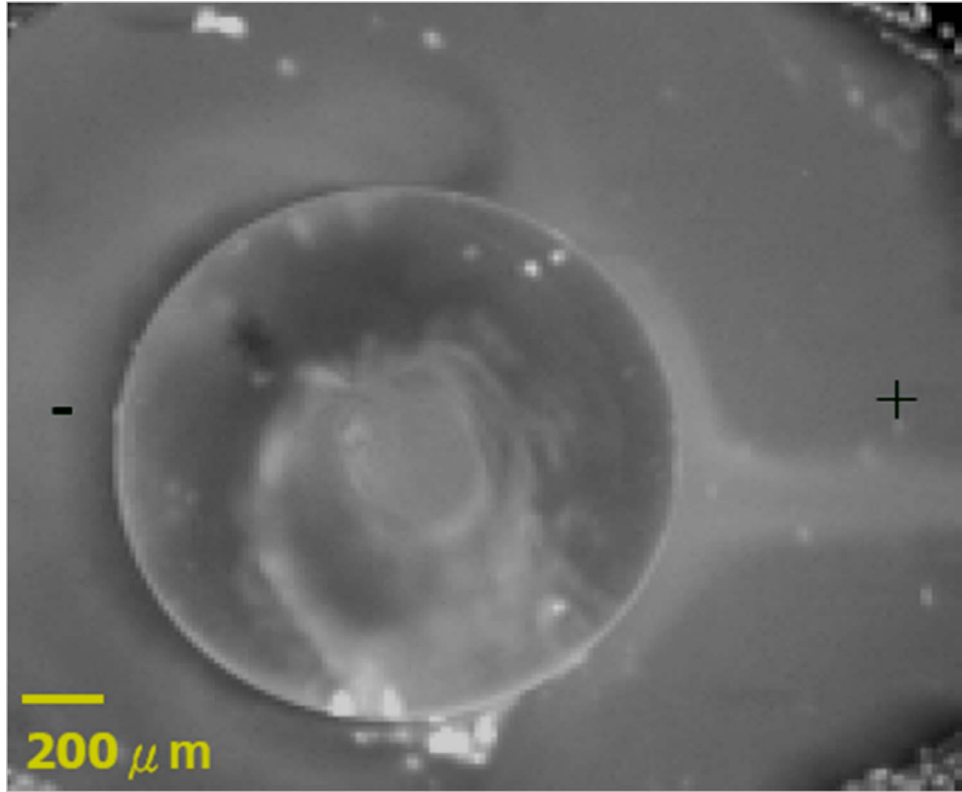


FIG. 6. The polar ejection for an anion exchange granule at 100 V/cm using co-ion Rhodamine B dyes (1  $\mu\text{M}$  in 10 mM citrate buffer at pH 4). The image is taken at 0.96 s.

Near the exit pole, when the concentrated counterions exceeds  $\delta$ , diffusion can no longer arrest the electromigration flux away from the pole, giving rise to a charge ejection. This ionic jet has a large electromigration flux density:  $j_+(r) \sim (DF/RT)CE[1 - (a/r)^3]$  (which synchronizes the electric field around the insulated particle. Because the flux at any cross section of the radius  $R(r)$  of the jet is sustained by the flux at the periphery of the pole region at  $\delta$ ,  $R^2 j_+(r) = \delta^2 j_+(r=a+\delta)$ , we find

$$\frac{R}{a} = \frac{\sqrt{3}}{\Gamma^{3/4}} [1 - (a/r)^3]^{-1/2}, \quad (1)$$

with  $R$  approaching  $\delta/2$  at a distance of about  $5\delta$  from the surface. The profile in Eq. (1) and the length of the jet are favorably compared to the cone-jet image in Fig. 8 for the experimental

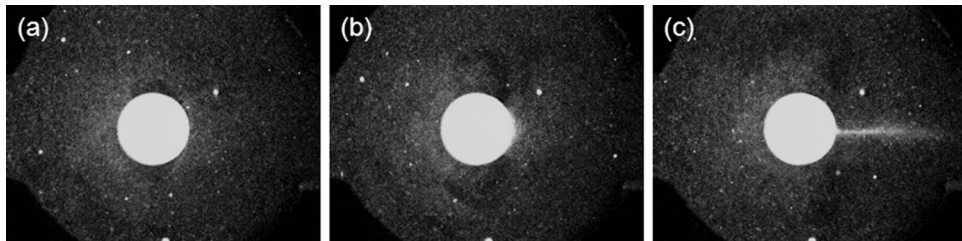


FIG. 7. The sequential images of microparticle concentration evolution for a cation exchange granule with a step change in the field to 100 V/cm using co-ion fluorescein-dye tagged microspheres in 10 mM Tris buffer (pH 8) at very low density ( $5.0 \times 10^6$  particles/mL). The images are taken at 0, 1.35, and 2.44 s.

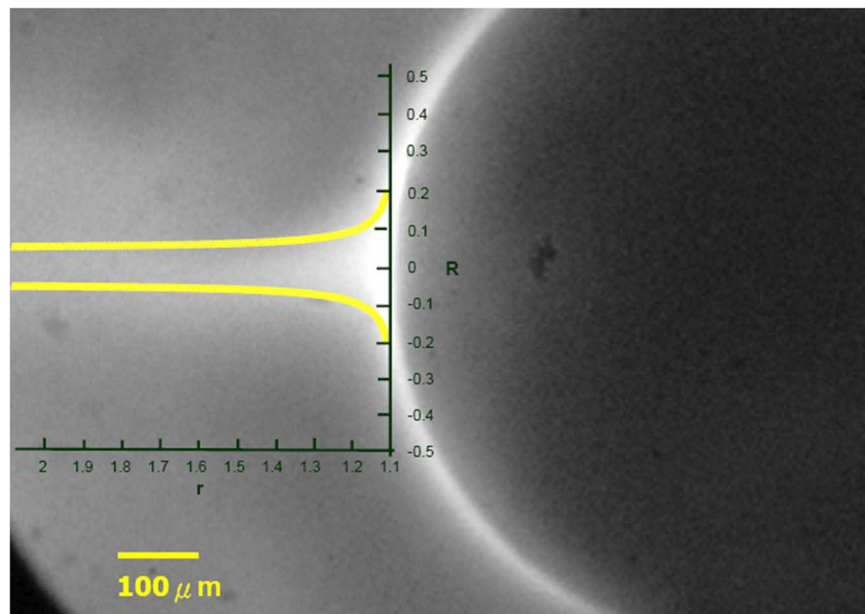


FIG. 8. Ion-concentrated ejection cone. The yellow profile is the theoretical prediction of Eq. (1) based on flux balance within the two bounding pole field lines.

condition of  $\Gamma=100$ , confirming the important gating role of the field critical point at the exit pole. This concentration phenomenon is occurring at a time scale of 1 s, which is much faster than the diffusive time scale due to concentration gradient, which is of the order of  $10^2$  s for the size of the granule used. In fact, the ratio of diffusion time to electromigration time scales is measured by the parameter  $\Gamma=FEd/ET$  which is of the order of  $10^2$ . Therefore, only electromigration is considered in Eq. (1).

- <sup>1</sup>Z. Gagnon and H.-C. Chang, *Electrophoresis* **26**, 3725 (2005).
- <sup>2</sup>M. Suzuki, T. Yasukawa, Y. Mase, D. Oyamatsu, H. Shiku, and T. Matsue, *Langmuir* **20**, 11005 (2004).
- <sup>3</sup>T. Bellini, F. Mantegazza, V. Degiorgio, R. Avallone, and D. A. Saville, *Phys. Rev. Lett.* **82**, 5160 (1999).
- <sup>4</sup>H. A. Pohl, *Dielectrophoresis* (Cambridge University Press, Cambridge, 1978).
- <sup>5</sup>S. S. Dukhin, *Adv. Colloid Interface Sci.* **35**, 173 (1991).
- <sup>6</sup>S. Tsukahara, T. Sakamoto, and H. Watarai, *Langmuir* **16**, 3866 (2000).
- <sup>7</sup>S. Basuray and H.-C. Chang, *Phys. Rev. E* **75**, 060501 (2007).
- <sup>8</sup>E. Brunet and A. Ajdari, *Phys. Rev. E* **73**, 056306 (2006).
- <sup>9</sup>N. G. Green, A. Ramos, A. Gonzalez, H. Morgan, and A. Castellanos, *Phys. Rev. E* **66**, 026305 (2002); N. G. Green, A. Ramos, A. Gonzalez, H. Morgan, and A. Castellanos, *ibid.* **61**, 4011 (2000); A. Gonzalez, A. Ramos, N. G. Green, A. Castellanos, and H. Morgan, *ibid.* **61**, 4019 (2000).
- <sup>10</sup>M. Z. Bazant and T. M. Squires, *Phys. Rev. Lett.* **92**, 066101 (2004).
- <sup>11</sup>Y. Ben and H.-C. Chang, *J. Fluid Mech.* **461**, 229 (2002); Y. X. Ben, E. A. Demekhin, and H.-C. Chang, *J. Colloid Interface Sci.* **276**, 483 (2004).
- <sup>12</sup>C. T. O'Konski, *J. Phys. Chem.* **64**, 605 (1960).
- <sup>13</sup>D. Stein, M. Kruijthof, and C. Dekker, *Phys. Rev. Lett.* **93**, 035901 (2004).
- <sup>14</sup>F. C. Leinweber and U. Tallarek, *J. Phys. Chem. B* **109**, 21481 (2005); U. Tallarek, F. C. Leinweber, and I. Nischang, *Electrophoresis* **26**, 391 (2005).
- <sup>15</sup>Y.-C. Wang, A. L. Stevens, and J. Y. Han, *Anal. Chem.* **77**, 4293 (2005).
- <sup>16</sup>H.-C. Chang, *AIChE J.* **53**, 2486 (2007); D. Hou, S. Maheshwari, and H.-C. Chang, *Biomicrofluidics* **1**, 014106 (2007); I.-F. Cheng, H.-C. Chang, D. Hou, and H.-C. Chang, *ibid.* **1**, 021503 (2007).
- <sup>17</sup>Laboratory Chemicals and Analytical Reagents (Fluka/Riedel-de Haen Catalogue, Switzerland, 2007/2008), p. 1214.